Supporting Information

Convergent Modulation of CHA Zeolites by Substituted Phenols and Ammonium Salts

Yanpeng Chen, [a,b] Mei Hong, * [a] Rongshu Zhu, * [b] and Shihe Yang * [a]

[a] Y. Chen, Prof. M. Hong, Prof. S. Yang

Guangdong Provincial Key Laboratory of Nano-Micro Materials Research

School of Advanced Materials

Peking University Shenzhen Graduate School (PKUSZ), Shenzhen 518055, P.R. China

hongmei@pku.edu.cn (M. Hong), chsyang@pku.edu.cn (S. Yang).

[b] Y. Chen, Prof. R. Zhu

State Key Laboratory of Urban Water Resource and Environment

Shenzhen Key Laboratory of Organic Pollution Prevention and Control

School of Eco-Environment

Harbin Institute of Technology Shenzhen, Shenzhen, 518055, P.R. China.

rszhu@hit.edu.cn (R. Zhu).

Experimental Procedures

Materials. All chemicals were used as-received. Aluminum hydroxide (AR, Macklin), JN-30 silica sol (30 wt.% SiO_2, Guangzhou Suixin Chemical Co., Ltd), Phenol (99 %, Aladdin), and potassium hydroxide (95 %, Aladdin) were used in the synthesis of zeolites. Substituted phenols including *p*-Nitrophenol (98 %, Macklin), *p*-Chlorophenol (99 %, Aladdin), 4-Fluorophenol (99 %, Aladdin), 4-Aminophenol (96 %, Energy Chemical), *p*-Cresol (99 %, Energy Chemical), Hydroquinone (99 %, Energy Chemical), 4-Methoxyphenol (98 %, Energy Chemical), and ammonium salts including Ammonium fluoride (98 %, Energy Chemical), Ammonium sulfate (99.99 %, Aladdin), Ammonium chloride (99.5 %, Aladdin) as mild in-situ etchant, denoted as Ω, have been added during zeolite synthesis.

Synthesis of CHA zeolites using phenolic compounds. The synthesis of CHA zeolites using phenolic compounds follows our previously reported procedure[12], with a modification involving the replacement of phenol with *para*-substituted phenols. The *p*-substituent functional groups include -NO_2, -Cl, -F, -H, -NH_2, -CH_3, -OH, and -OCH_3. The specific phenolic compounds used are as follows: *p*-Nitrophenol (NO_2phe), *p*-Chlorophenol (Clphe), 4-Fluorophenol (Fphe), Phenol (Hphe), 4-Aminophenol (NH_2phe), *p*-Cresol (CH_3phe), Hydroquinone (OHphe), 4-Methoxyphenol (CH_3Ophe). The detailed procedure involves heating a mixture of aqueous solution of aluminum hydroxide and potassium hydroxide at 100 °C with stirring until a clear solution was obtained. After cooling to room temperature, a calculated amount of JN-30 silica sol and the phenolic compound (Ω) were added sequentially and thoroughly mixed for 10 minutes to ensure homogeneity. The mixture was then placed in a stainless-steel autoclave lined with polytetrafluoroethylene (PTFE). To study the influence of different phenolic compounds, the final gel composition was adjusted in molar ratios to KOH : $Al(OH)_3$: SiO_2 : Ω : H_2O = 7 : 4 : 10 : n (n=0-6) : 150. The gel was then aged for 24 h at room temperature with stirring at 20 rpm. After aging, the temperature was increased from room temperature to 160 °C at a rate of 10 °C/min and the hydrothermal synthesis was carried out for 96 h at 10 rpm. The product was then washed several times

with deionized water by centrifugation and dried at 80 °C for 12 h to obtain the potassium-form zeolite (K-CHA), designated as K-nΩ (K-nNO_2phe, K-nClphe, K-nFphe, K-nHphe, K-nNH_2phe, K-nCH_3phe, K-nOHphe, K-nOCH_3phe).

Synthesis of CHA zeolites using ammonium salts. The synthesis follows the same hydrothermal synthesis as that using phenolic compounds except that ammonium salts was added instead. In a typical preparation, 1.45 g potassium hydroxide was dissolved in 4.33 g deionized water and heated to 100 °C in an oil bath. Then 1.04 g aluminum hydroxide was added to the potassium hydroxide solution and stirred under heat for 3 h until a clear solution was obtained. After cooling to room temperature, 6.68 g JN-30 silica sol was added and stirred for 10 minutes, followed by the addition of specified amounts of ammonium salts (NH_4F, $(NH_4)_2SO_4$, or NH_4Cl). The final gel, with a molar composition of KOH : $Al(OH)_3$: SiO_2 : ammonium salt : H_2O = 7 : 4 : 10 : n (n=0-6) : 150, was transferred to a homogeneous reactor and aged at room temperature for 24 h at 20 rpm. The temperature was then increased to 160 °C at a rate of 10 °C/min and kept for 4 days at 10 rpm. Finally, the product was cooled to room temperature with cold water, washed at least three times with deionized water and dried at 80 °C for 12 h to obtain the zeolite product named K-nNH_4X (K-nNH_4F, K-n$(NH_4)_2SO_4$ and K-nNH_4Cl).

Cation exchange. The obtained K-CHA samples were first exchanged into its NH_4^+ form by mixing with 2.5 mol L^{-1} $(NH_4)_2SO_4$ solution (1 g zeolite in 30 mL solution) at 80 °C for 8 h, denoted as NH_4-CHA. H-form zeolite was prepared from calcination of NH_4-CHA at 550 °C for 6 h with a ramping rate of 3 °C/min, named as H-CHA. Cu-CHA zeolite catalyst was synthesized by an ion-exchange process in which 1 g of H-CHA zeolite was added to a 50 mL aqueous solution of $Cu(NO_3)_2$ at molar concentrations of 0.1 mol L^{-1}. The mixture was then heated in an oil bath at 80 °C for 8 h. After ion exchange, the material was washed three times with deionized water, dried at 80 °C for 12 h and then calcined at 550 °C for 6 h.

Post synthetic dissolution test. Post-treatment of SSZ-13 was conducted on K-4.0Hphe zeolite as the parent sample, which was etched in aqueous suspension containing 1 g zeolite in 30 mL solution with different etchant concentrations.

Materials Characterizations. Powder X-ray diffraction (XRD) patterns were recorded using a Rigaku D/Max-2200 PC diffractometer in the diffraction angle range 2θ = 4°-55° with Cu Kα radiation (λ = 1.5418 Å) at 40 kV, 40 mA. The relative crystallinity was estimated with the intensities of peaks at 20.5° in the XRD patterns of each zeolite sample normalized to the best K-CHA in each series as a standard. Scanning electron microscopy (SEM) was measured by a JEOL JSM-7800F electron microscope operated at 5.0 kV. An Oxford Instruments X-Max^N Falcon energy dispersive X-ray spectroscopy (EDX) was used to analyze elements contained in the samples, based on which the Si/Al ratios of the as synthesized samples were acquired. Transmission electron microscopy (TEM) and TEM-EDX were performed on a JEM-3200FS field emission source transmission electron microscope operated at 300 kV. The zeolite samples were embedded in Spurr epoxy resin and ultramicrotomed to a thickness of 80 nm for TEM measurements. Textural properties of the samples were obtained by nitrogen adsorption-desorption isotherms at -196 °C using a Micromeritics Tristar II 3020 v1.03 analyzer. The BET surface areas (S_{BET}) were obtained from N_2 adsorption isotherm in a relative pressure range of 0.05–0.30; micropore volumes (V_{micro}) were obtained from a *t*-plot method; total pore volume (V_{total}) were calculated as the amount of N_2 adsorbed at P/P_0 = 0.98, and average mesopore volume (V_{meso}) was calculated as the difference between the total pore volume and the micropore volume. The samples were calcined at 550 °C for 6 h and then degassed at 300 °C for at least 3 h before measurements. The ^{29}Si and ^{27}Al magic-angle spinning nuclear magnetic resonance (MAS NMR) spectra of the calcined zeolite powders were recorded at 199.13 and 156.25 MHz, respectively, using a zirconia rotor of 4 mm diameter, on an Agilent 600 DD2 spectrometer with magnetic field strength 14.1 T. The rotor was spun with dry air at 8 kHz. The spectra were accumulated with 4 μs pulses, 3 s recycle delay, 1024 scans for ^{29}Si MAS NMR and 3.6 μs pulses, 1 s recycle delay, 128 scans for ^{27}Al MAS NMR. The Si signal of tetramethylsilane (TMS) at 0 ppm or Al signal of $AlCl_3$ at 0.9 ppm was used as the reference of ^{29}Si or ^{27}Al chemical shift respectively. The ^{19}F MAS NMR spectra was recorded on an Agilent 600 DD2 spectrometer (Agilent, USA, magnetic field strength 14.1 T) at resonance frequency of 564.21 MHz. The powder

samples were placed in a pencil-type zirconia rotor of 4.0 mm. The spectra were obtained at a spinning speed of 8 kHz. The experiment used a relaxation delay of 3 s and an approximately 90-degree pulse (2.6 μs). The F signal of CCl_3F was used as the reference of ^{19}F chemical. Raman investigations were performed on Renishaw Qontor Raman Spectrometer (Invia) with the excitation wavelength of 532 nm, laser power of 5% and a 100× objective. Thermogravimetric analyses (TGA) was carried out on a Shimadzu TGA-50 analyzer. The sample was heated from 25 °C to 600 °C with a heating ramp of 5 °C/min under N_2 (flow rate: 40 mL/min). The reducibility of the catalysts was evaluated by programmed temperature reduction with hydrogen (H_2-TPR, Micromeritics AutoChem1 II 2920): 100 mg catalysts in a U-shaped quartz tube, pretreated by drying from room temperature to 300 °C at a rate of 10 °C/min and purging in He flow of 30 ml/min for 2 h, were cooled to 50 °C followed by exposure to 10 vol.% H_2/Ar mixture flow of 30 ml/min and heating to 600 °C at a rate of 10 °C/min.

Catalytic test. The NH_3-SCR reaction was carried out on a fixed-bed reactor. 100 mg of catalyst was added to a quartz tube with inner diameter of 6 mm. A total flow of 100 mL/min simulated diesel vehicle exhaust with 400 ppm NO_x, 400 ppm NH_3, 5% O_2, and N_2 as the balance gas was employed as feed, corresponding to a gas hourly space velocity (GHSV) of approximately 43,200 h^{-1}. A flue gas analyzer (Thermo model 42i) was used to measure the concentration of nitrogen oxides in the import and export gases. For the catalyst activity evaluation the reaction temperature ramped from 50 to 550 °C at a rate of 3 °C/min, and sampling was taken at an interval of every 5 °C. The NO_x conversion was calculated according to Eq. (1). Long-time stability test of the catalyst was carried out by maintaining the reaction at 300 °C for given period of time.

$$\eta = \frac{c(NO_x)_{in} - c(NO_x)_{out}}{c(NO_x)_{in}} \times 100\,\% \qquad \text{Eq. (1)}$$

Results and Discussion

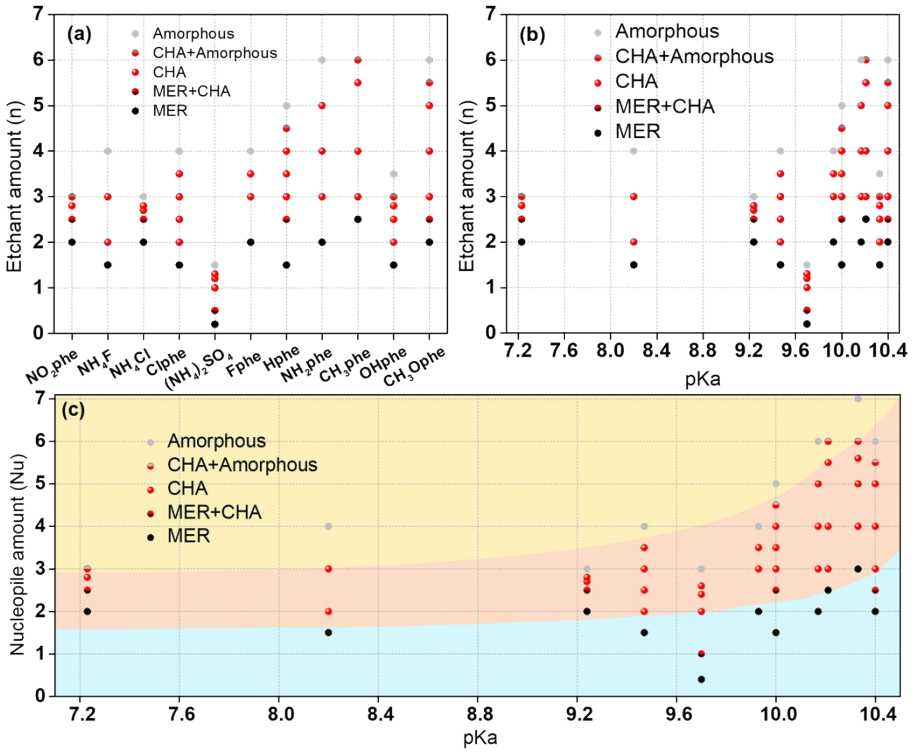

Figure S1. Phase modulation by the etchant amount and property combination. (a) Correlation between the etchant and the modulated phase of the zeolite products, (b) effect of etchant amount and pKa value on the final zeolite phase. (c) effect of nucleophile amount, Nu, defined as the etchant amount (n) multiplied by the number of dissociable proton (N_{H+}), and pKa value on the final zeolite phase.

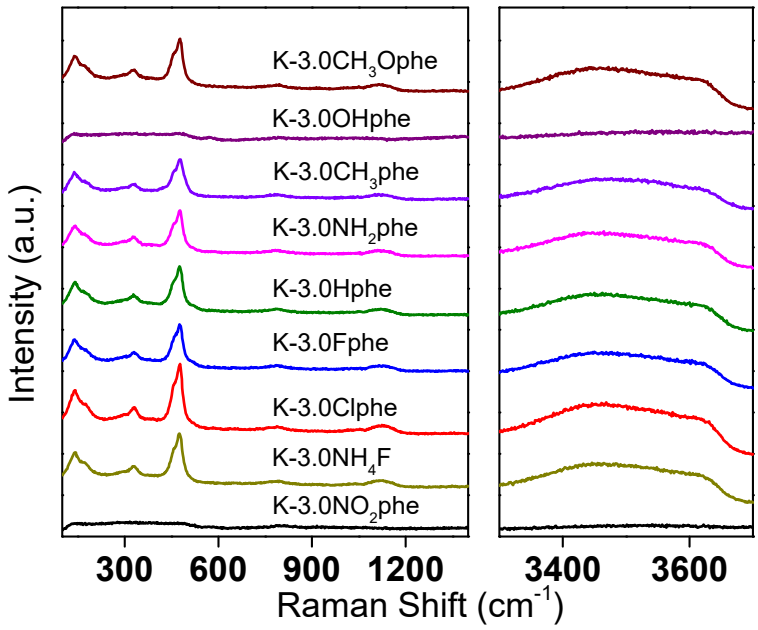

Figure S2. Raman spectra of as-synthesized K-3.0Ω zeolites.

Table S1. Effect of added etchant and their amount on the as-synthesized zeolite phase represented by the three-letter code of MER or CHA, while * represents amorphous phase. The conditions that lead to successful synthesis of pure CHA zeolites are highlighted in yellow.

pKa	Ω	n amount (n=10Ω/SiO_2)																	
		0.2	0.5	1	1.2	1.3	1.5	1.8	2	2.5	2.7	2.8	3	3.5	4	4.5	5	5.5	6
7.23	NO_2phe								MER	MER+ CHA		CHA	CHA+*						
8.2	NH_4F						MER		CHA				CHA		*				
9.24	NH_4Cl								MER	MER+ CHA	CHA	CHA	*						
9.47	Clphe						MER		CHA	CHA			CHA	CHA	*				
9.7	$(NH_4)_2SO_4$	MER	MER+ CHA	CHA	CHA	CHA	*												
9.93	Fphe								MER				CHA	CHA	CHA+*				
10.00	Hphe			MER						MER+ CHA			CHA	CHA	CHA	CHA	*		
10.17	NH_2phe								MER				CHA		CHA		CHA		*
10.21	CH_3phe									MER			CHA		CHA			CHA	CHA+*
10.33	OHphe						MER		CHA	CHA		CHA	CHA+*	*					
10.40	CH_3Ophe								MER	MER+ CHA			CHA		CHA		CHA	CHA+*	*

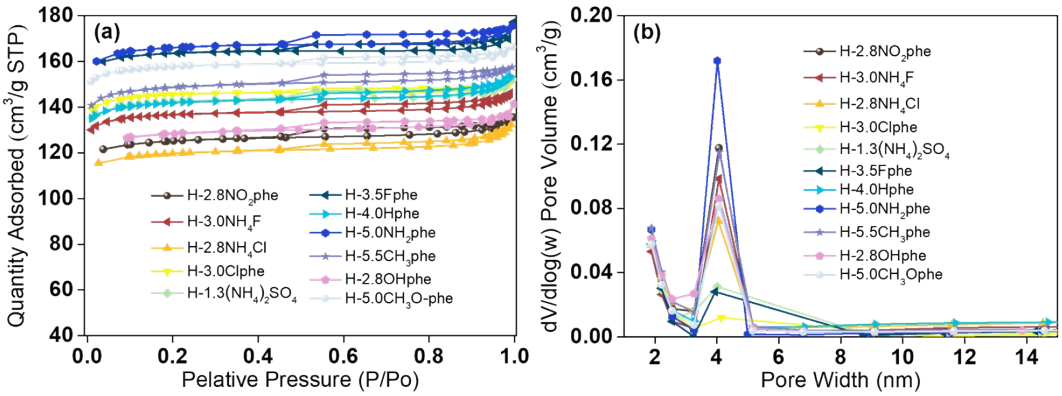

Figure S3. (a) Nitrogen adsorption-desorption isotherms at -196 °C and (b) BJH pore size distribution of H-CHA zeolites mediated with different phenolic compounds or ammonium salts.

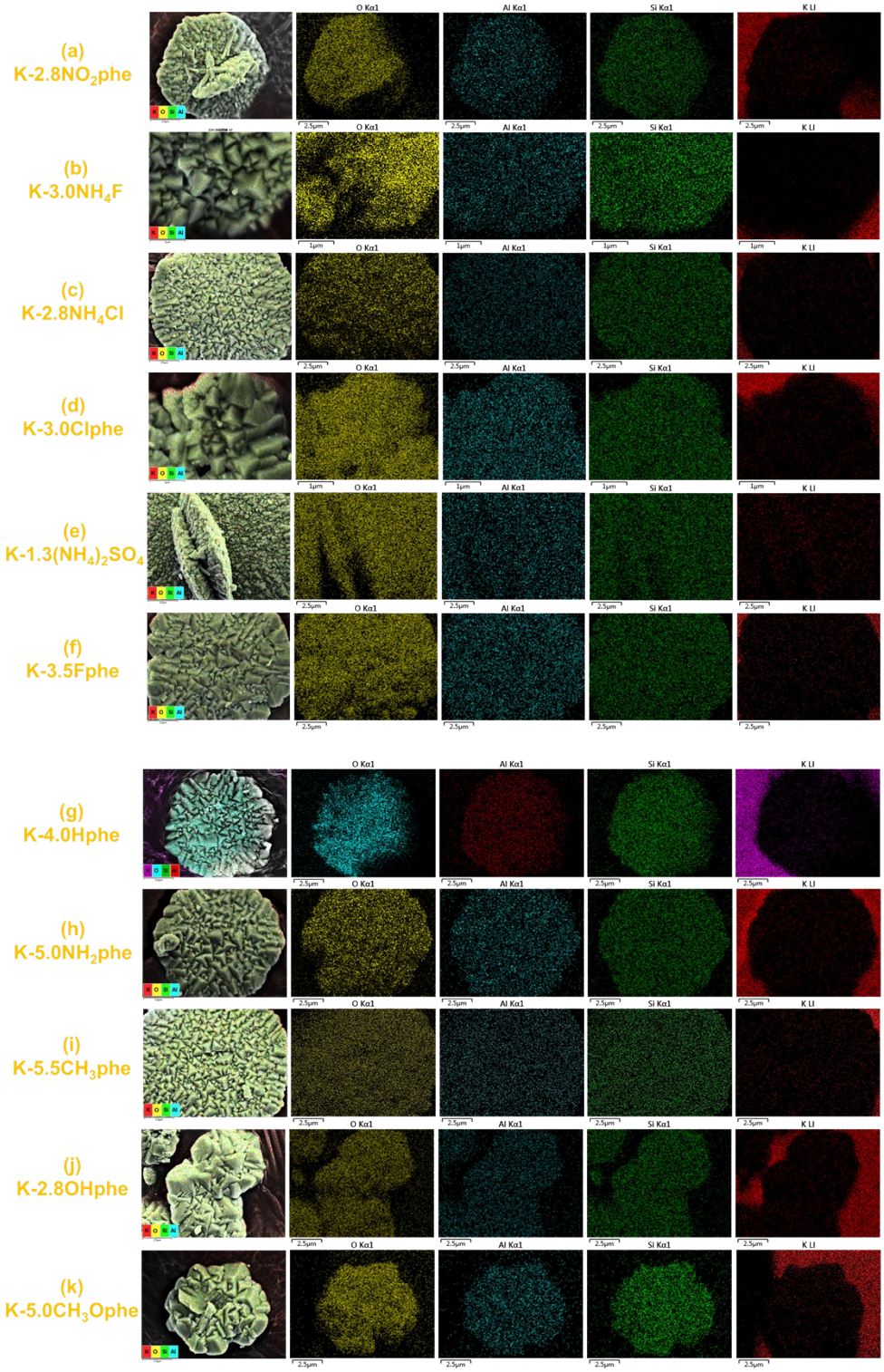

Figure S4. SEM images and EDX mappings of CHA zeolites mediated with different phenolic compounds or ammonium salts.

Table S2. Elemental contents of the CHA zeolites mediated with different amount of ammonium salt or substituted phenol addition analyzed by EDX mapping, and the calculated Si/Al ratios.

Sample	pKa	K At%	O At%	Si At%	Al At%	Si/Al
K-2.8NO_2phe	7.23	4.9	65.4	21.0	8.7	2.41
K-3.0NH_4F	8.2	6.8	61.7	22.2	9.3	2.39
K-2.8NH_4Cl	9.24	6.4	65.4	19.7	8.5	2.32
K-3.0Clphe	9.47	5.1	62.5	22.6	9.8	2.31
K-1.3$(NH_4)_2SO_4$	9.7	6.1	66.3	19.6	8.0	2.45
K-3.5Fphe	9.93	3.5	68.6	19.7	8.2	2.40
K-4.0Hphe	10.00	2.2	67.4	21.1	9.3	2.27
K-5.0NH_2phe	10.17	4.4	69.2	18.5	8.0	2.31
K-5.5CH_3phe	10.21	6.0	67.7	18.5	7.8	2.37
K-2.8OHphe	10.33	5.2	54.0	28.7	12.1	2.37
K-5.0CH_3Ophe	10.40	8.3	66.0	18.9	6.7	2.82

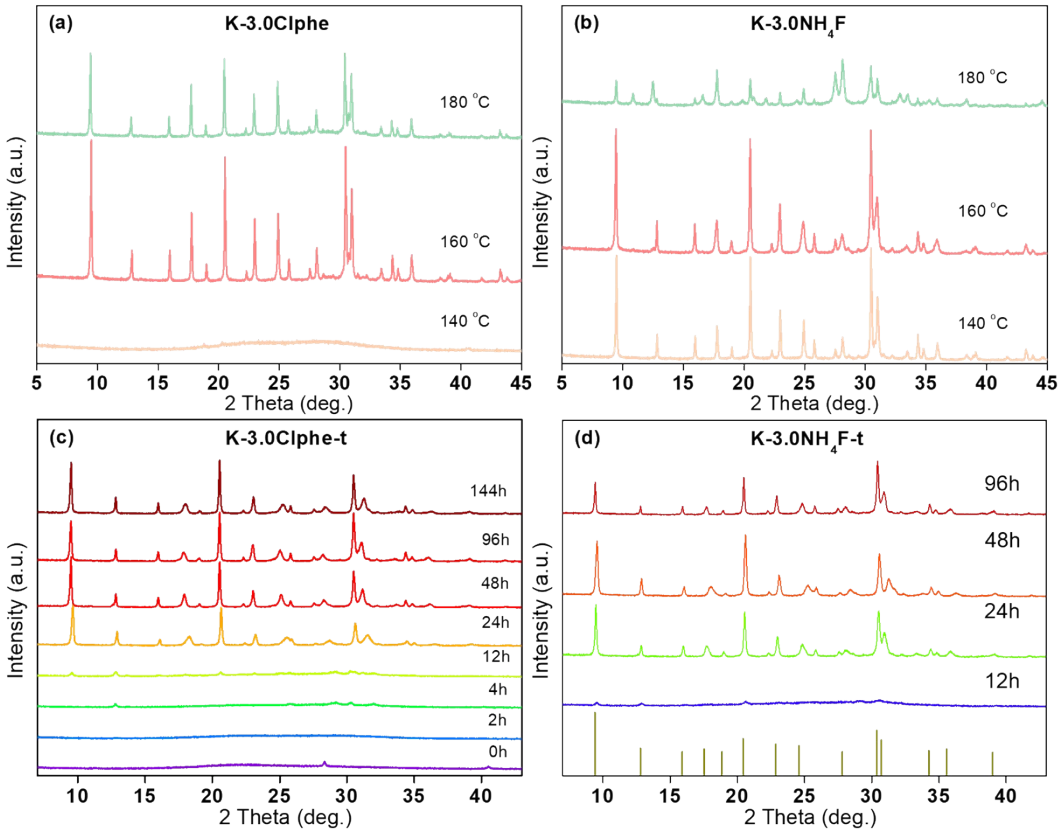

Figure S5. Effect of operation conditions including synthesis temperature and reaction time on the XRD patterns of the CHA zeolites. (a-b) synthesis temperature effect on (a) K-3.0Clphe and (b) K-3.0NH_4F crystallized for 96 h, (c-d) synthesis time effect on (c) K-3.0Clphe and (d) K-3.0NH_4F crystallized at 160 °C.

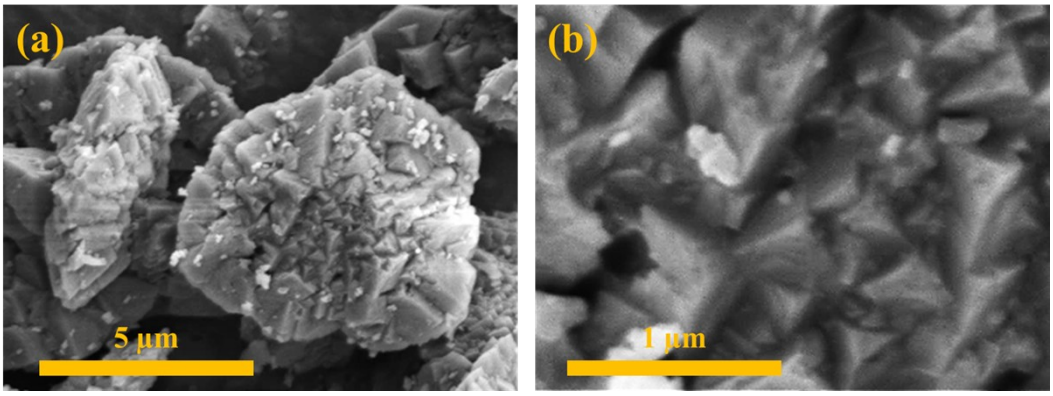

Figure S6. SEM images of K-3.5Clphe at different magnifications

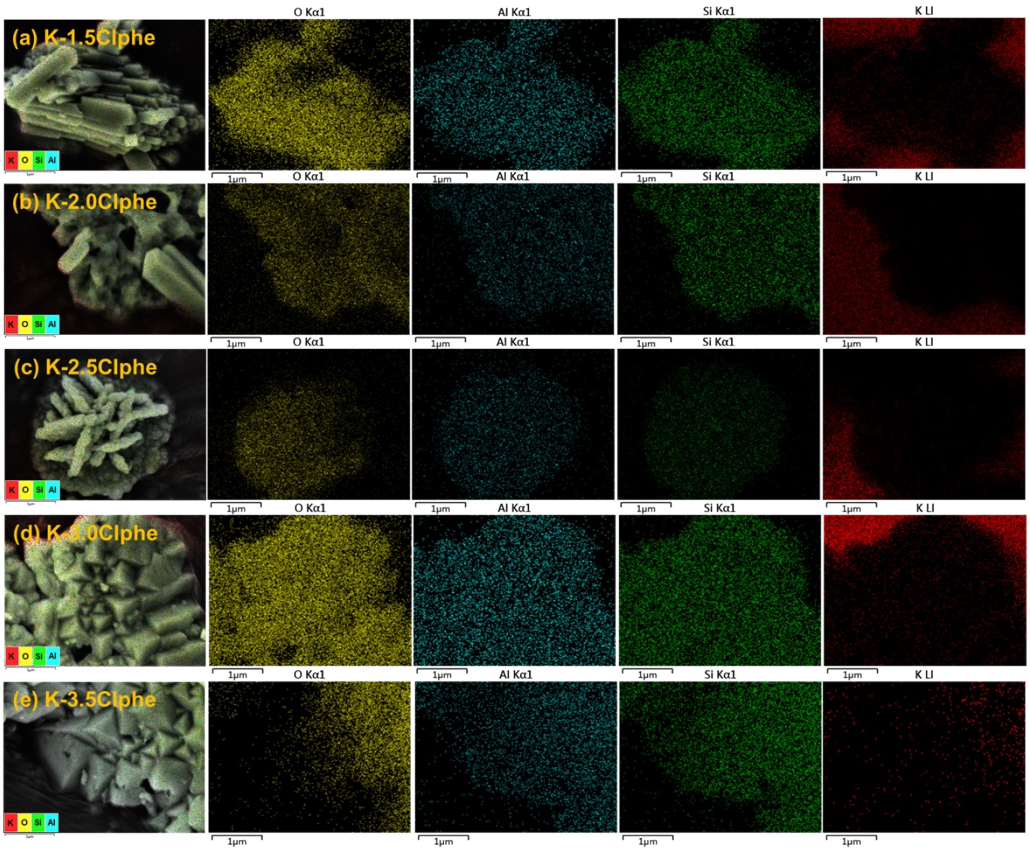

Sample name	K At%	O At%	Si At%	Al At%	Si/Al
K-1.5Clphe	5.2	62.4	22.5	9.9	2.27
K-2.0Clphe	7.1	61.5	21.7	9.7	2.24
K-2.5Clphe	6.6	61.8	22	9.6	2.29
K-3.0Clphe	5.1	62.5	22.6	9.8	2.31
K-3.5Clphe	6.4	62	22.9	8.7	2.63

Figure S7. SEM-EDX images and mappings of K-nClphe, and the corresponding elemental analysis

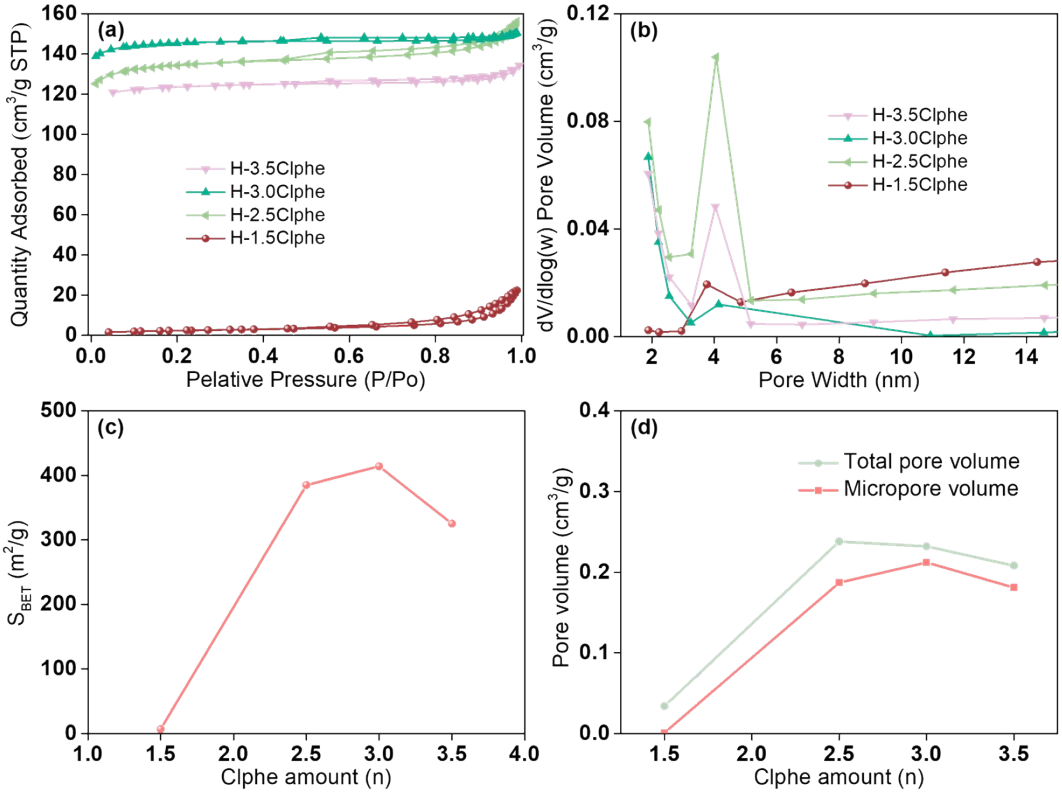

Figure S8. (a) Nitrogen adsorption-desorption isotherms at -196 °C, (b) BJH pore size distributions, (c) BET surface area, (d) total and micropore volume of series Clphe-mediated zeolites after ion exchange to their H-form, H-nClphe.

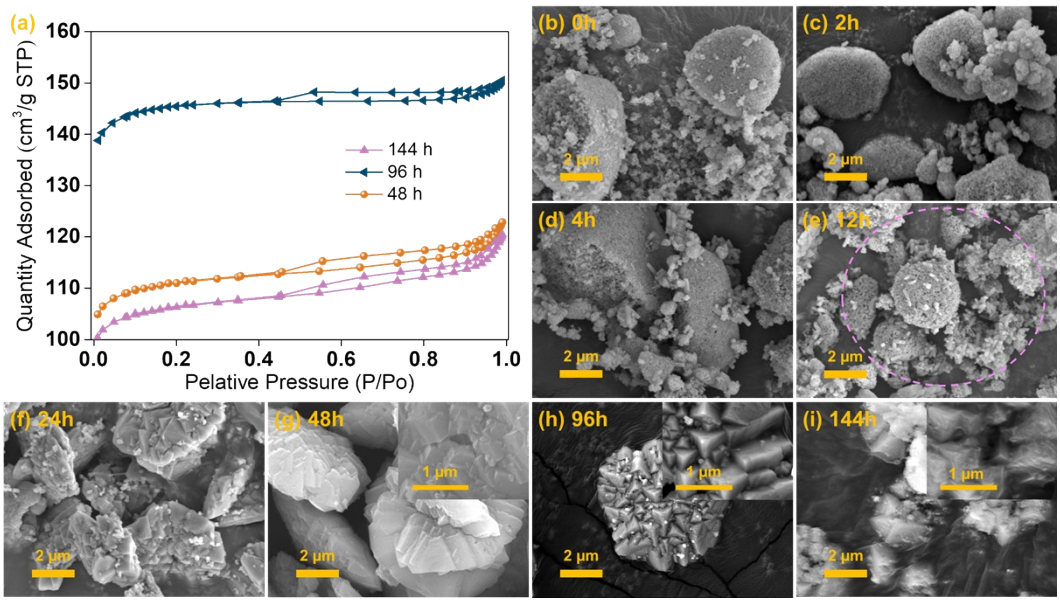

Synthesis time for K-3.0Clphe-t	BET Surface Area (m^2/g)	Micropore volume (cm^3/g)	Total pore volume of pores (cm^3/g)	Average pore width (nm)
144 h	304.11	0.15	0.18	2.43
96 h (standard)	413.70	0.21	0.23	2.24
48 h	317.40	0.16	0.19	2.37

Figure S9. Effect of synthesis time on the crystal properties of K-3.0Clphe-t showing N_2 adsorption-desorption isotherms of ion-exchanged H-form of H-3.0Clphe-t and the corresponding SEM images and textural properties. The circled SEM image show the emergence of CHA crystals at t = 12 h.

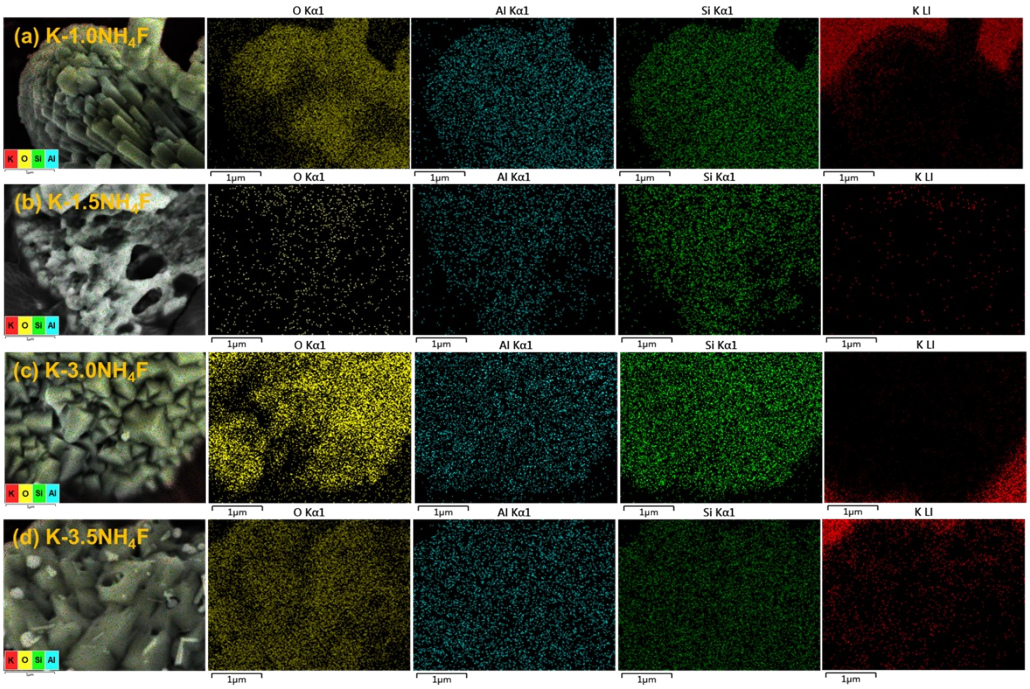

Sample name	K At%	O At%	Si At%	Al At%	Si/Al
K-1.5NH_4F	3.7	63.1	23.1	10.1	2.29
K-2.0NH_4F	8.2	61	21.5	9.3	2.31
K-3.0NH_4F	6.8	61.7	22.2	9.3	2.39
K-3.5NH_4F	6.1	62.1	22.6	9.3	2.43

Figure S10. SEM-EDX images and mappings of K-nNH_4F, and the corresponding elemental analysis

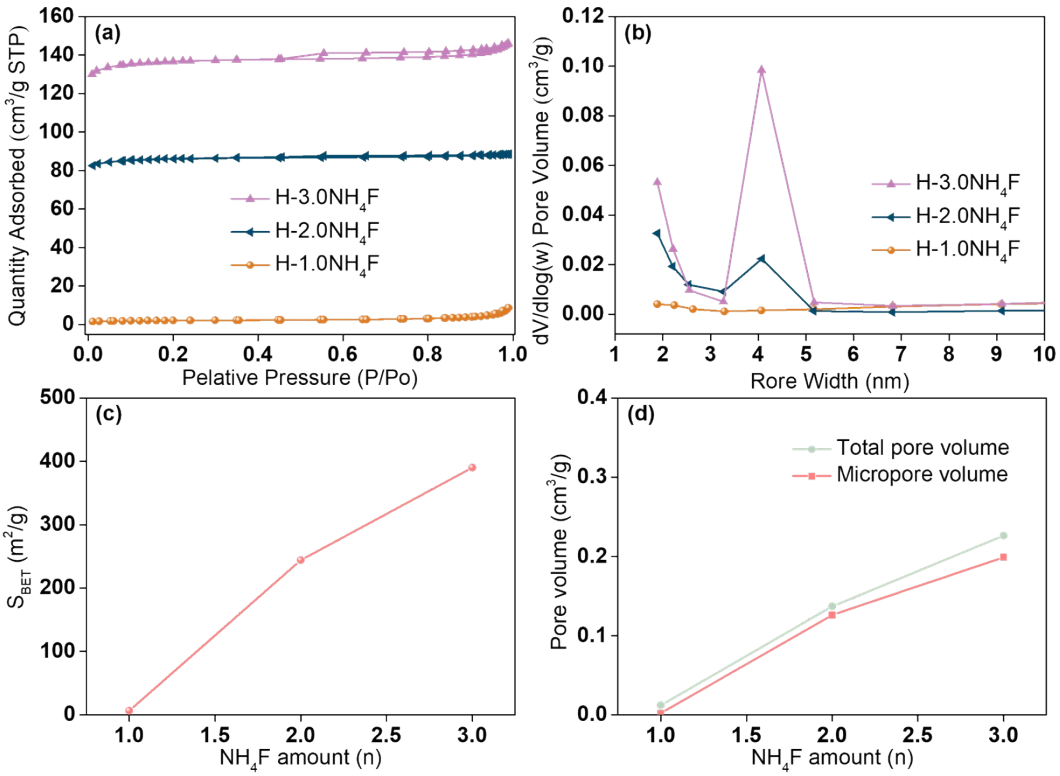

Figure S11. (a) Nitrogen adsorption-desorption isotherms at -196 °C and (b) BJH pore size distribution, (c) BET surface area, (d) total and micropore volume of the series NH_4F-mediated zeolites after ion exchange to their H-form, H-nNH_4F.

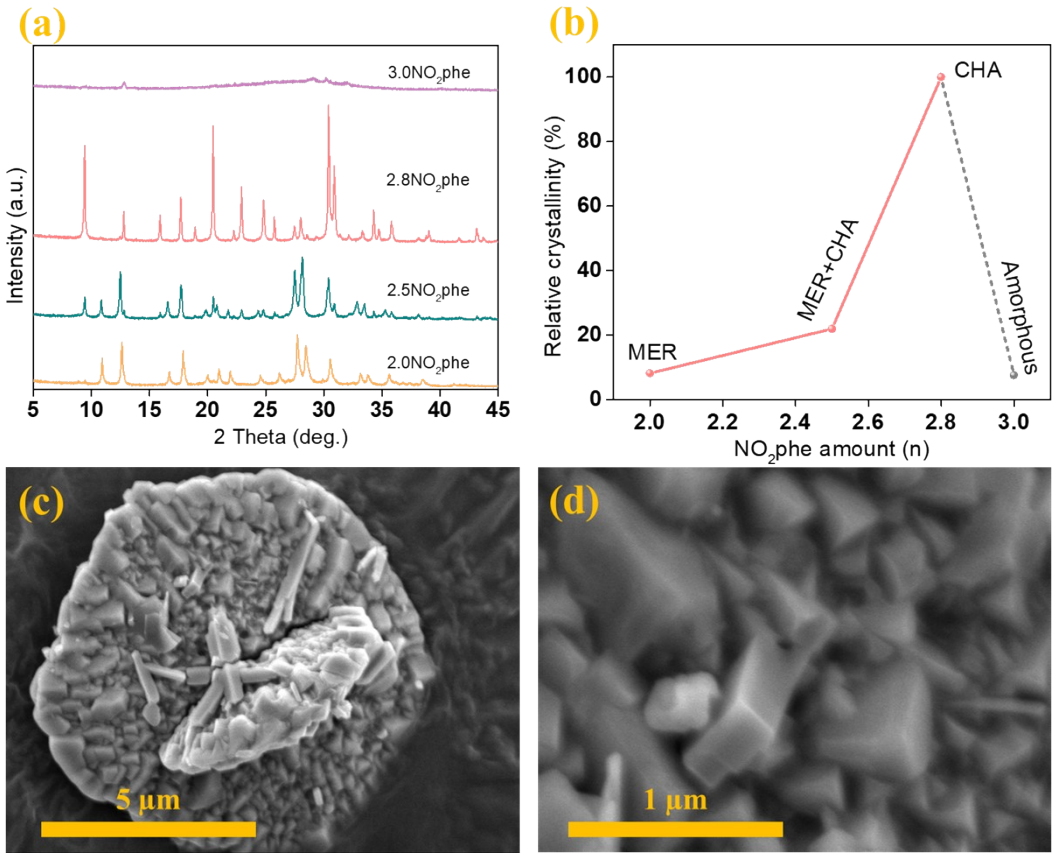

Figure S12. (a) XRD patterns of the as-synthesized K-nNO_2phe samples (n = 2.0, 2.5, 2.8, 3.0), and (b) the relative crystallinity profile of the CHA zeolites normalized to that of K-2.8NO_2phe as a function of added NO_2phe amount. (c-d) SEM images of the as-synthesized K-2.8NO_2phe sample, (c) presents a lower magnification overview, while (d) offers a higher magnification detail of the zeolite.

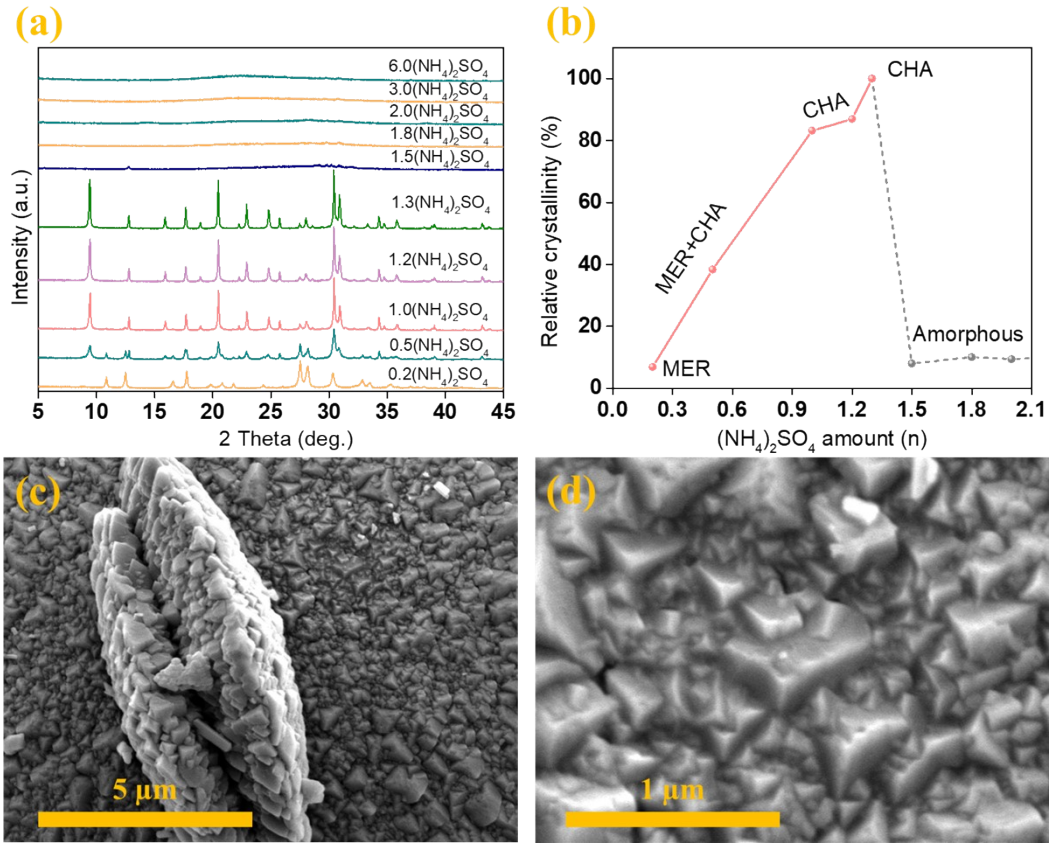

Figure S13. (a) XRD patterns of the as-synthesized K-n$(NH_4)_2SO_4$ samples (n = 0.2, 0.5, 1.0, 1.2, 1.3, 1.5, 1.8, 2.0, 3.0, 6.0), and (b) the relative crystallinity profile of CHA zeolites normalized to that of K-1.3$(NH_4)_2SO_4$ as a function of added $(NH_4)_2SO_4$ amount. (c-d) SEM images of the as-synthesized K-1.3$(NH_4)_2SO_4$ sample, (c) presents a lower magnification overview, while (d) offers a higher magnification detail of the zeolite.

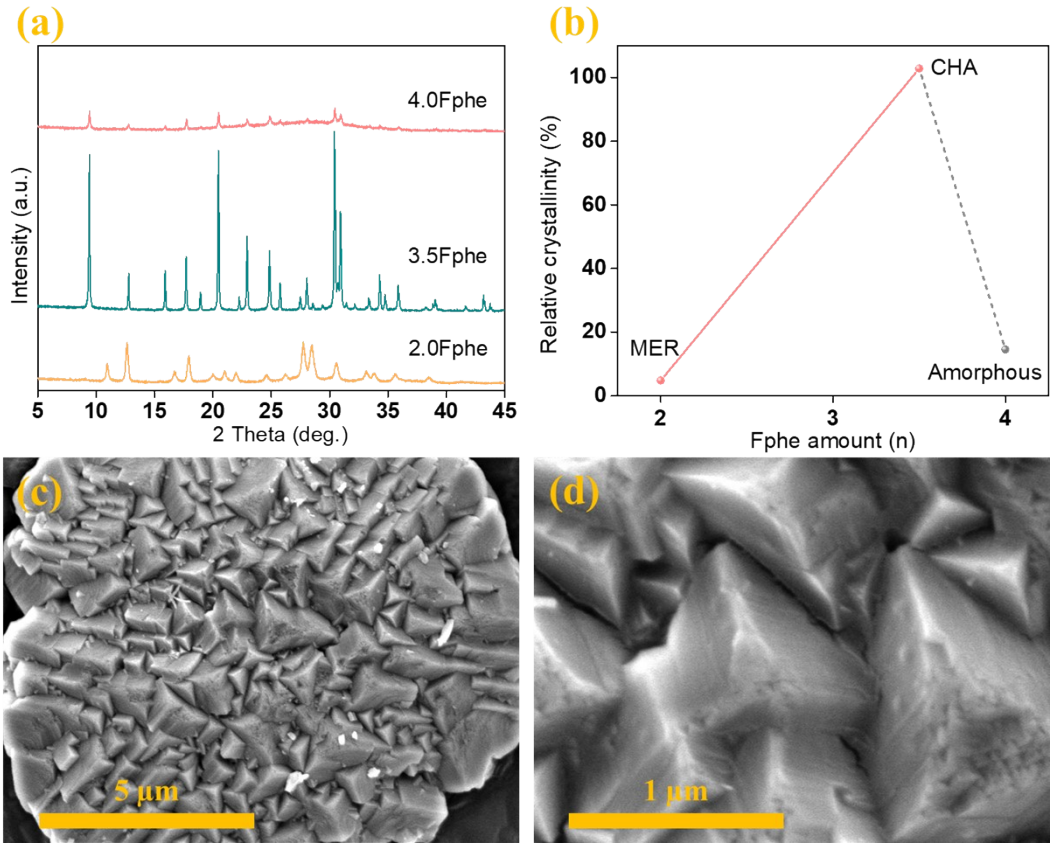

Figure S14. (a) XRD patterns of the as-synthesized K-nFphe samples (n = 2.0, 3.5, 4.0), and (b) the relative crystallinity profile of CHA zeolites normalized to that of K-3.5Fphe as a function of added Fphe amount. (c-d) SEM images of the as-synthesized K-3.5Fphe sample, (c) presents a lower magnification overview, while (d) offers a higher magnification detail of the zeolite.

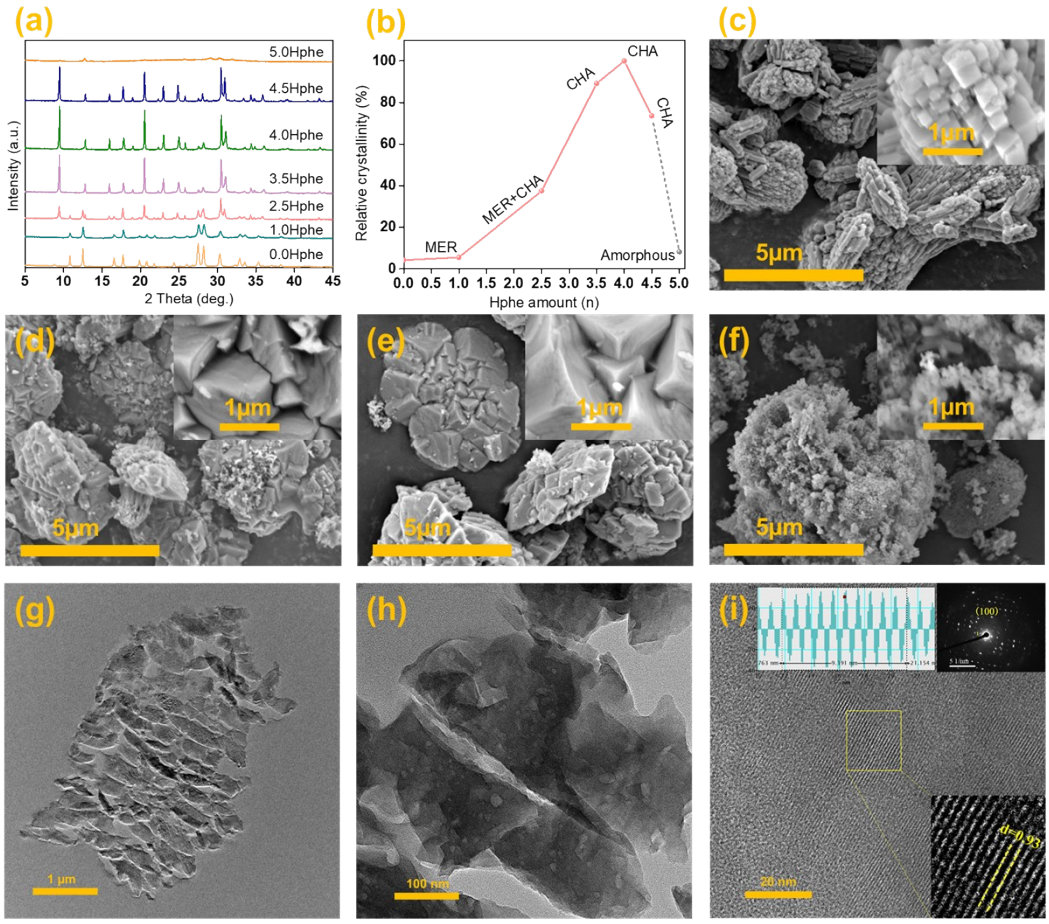

Figure S15. (a) XRD patterns of the as-synthesized K-nHphe samples (n = 0.0, 1.0, 2.5, 3.5, 4.0, 4.5, 5.0), and (b) the relative crystallinity profile of CHA zeolites normalized to that of K-4.0Hphe as a function of added Hphe amount. (c-f) SEM images of the as-synthesized K-nHphe samples: (c) K-1.0Hphe, (d) K-3.5Hphe, (e) K-4.0Hphe, (f) K-5.0Hphe; insets show magnified surface features. (g-i) TEM images of the K-4.0Hphe zeolite with (g-h) low-resolution, (i) high-resolution, insets show the selected-area electron diffraction (SAED) pattern with diffraction spots that can be indexed to CHA-type zeolite and lattice fringe spacing of 0.93 nm expected for the (100) planes. The crevices in the cross-sectional TEM images result from the ultramicrotomy action that slightly breaks the zeolite crystals.

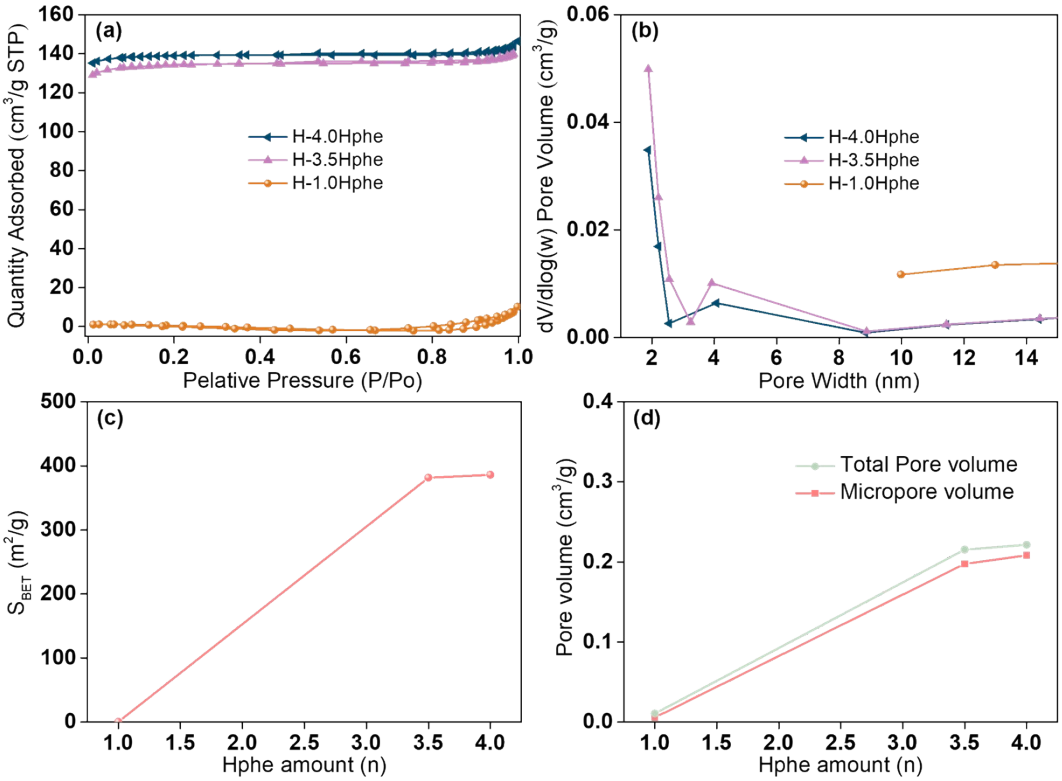

Figure S16. (a) Nitrogen adsorption-desorption isotherms at -196 °C and (b) BJH pore size distribution of phenol-mediated zeolites with different Hphe after ion exchange to their H-form. (c) BET surface area, (d) total and micropore volume of the series phenol-mediated zeolites after ion exchange to their H-form, H-nHphe.

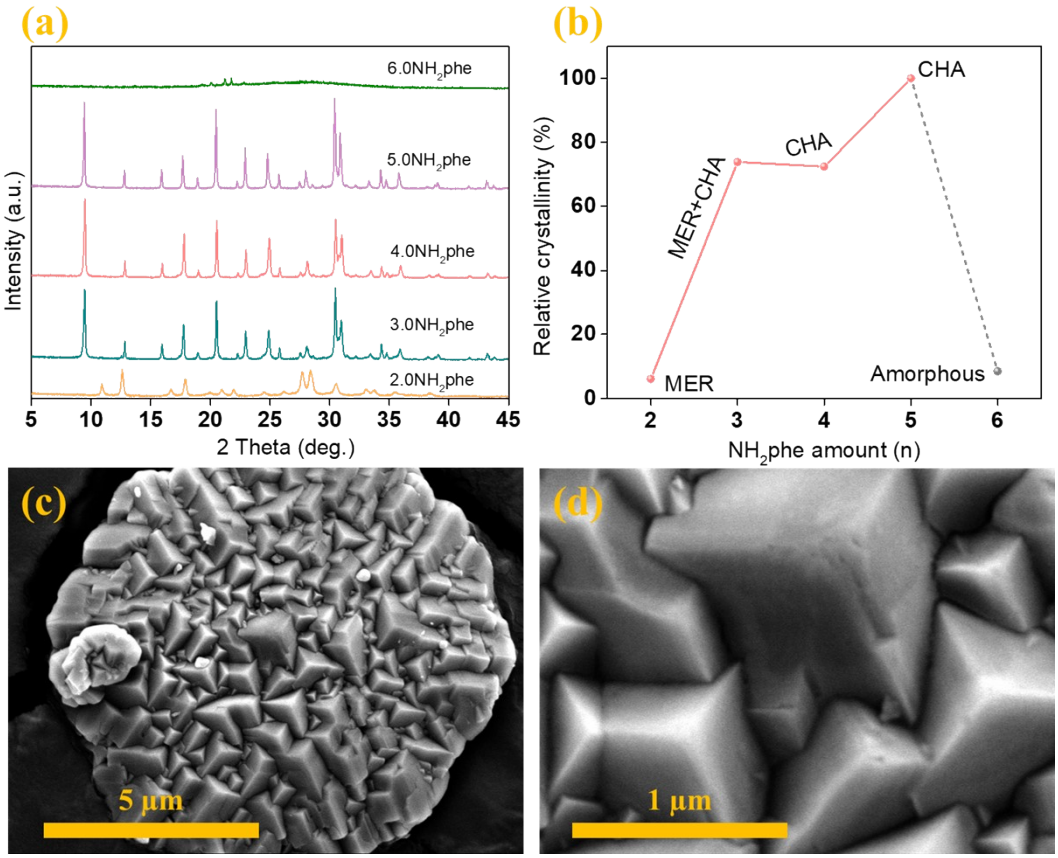

Figure S17. (a) XRD patterns of the as-synthesized K-nNH_2phe samples (n = 2.0, 3.0, 4.0, 5.0, 6.0), and (b) Relative crystallinity profile of CHA zeolites normalized to that of K-5.0NH_2phe as a function of added NH_2phe amount. (c-d) SEM images of the as-synthesized K-5.0NH_2phe sample, (c) presents a lower magnification overview, while (d) offers a higher magnification detail of the zeolite.

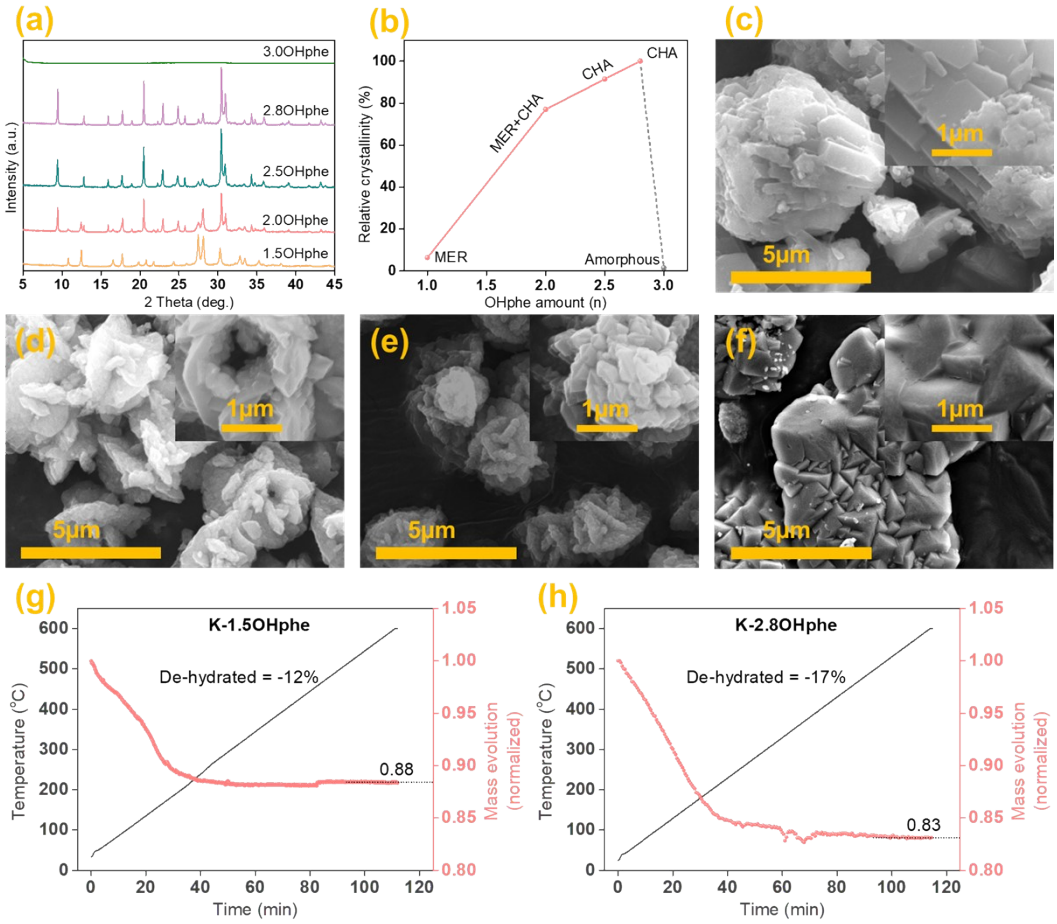

Figure S18. (a) XRD patterns of the as-synthesized K-nOHphe samples (n = 1.5, 2.0, 2.5, 2.8), and (b) the relative crystallinity profile of CHA zeolites normalized to that of K-2.8Hyd as a function of added hydroquinone amount. (c-f) SEM images of the as-synthesized K-nOHphe samples: (c) K-1.5OHphe, (d) K-2.0OHphe, (e) K-2.5OHphe, (f) K-2.8OHphe; insets show magnified surface features. (g-h) TGA profiles of (g) K-1.5OHphe and (h) K-2.8OHphe

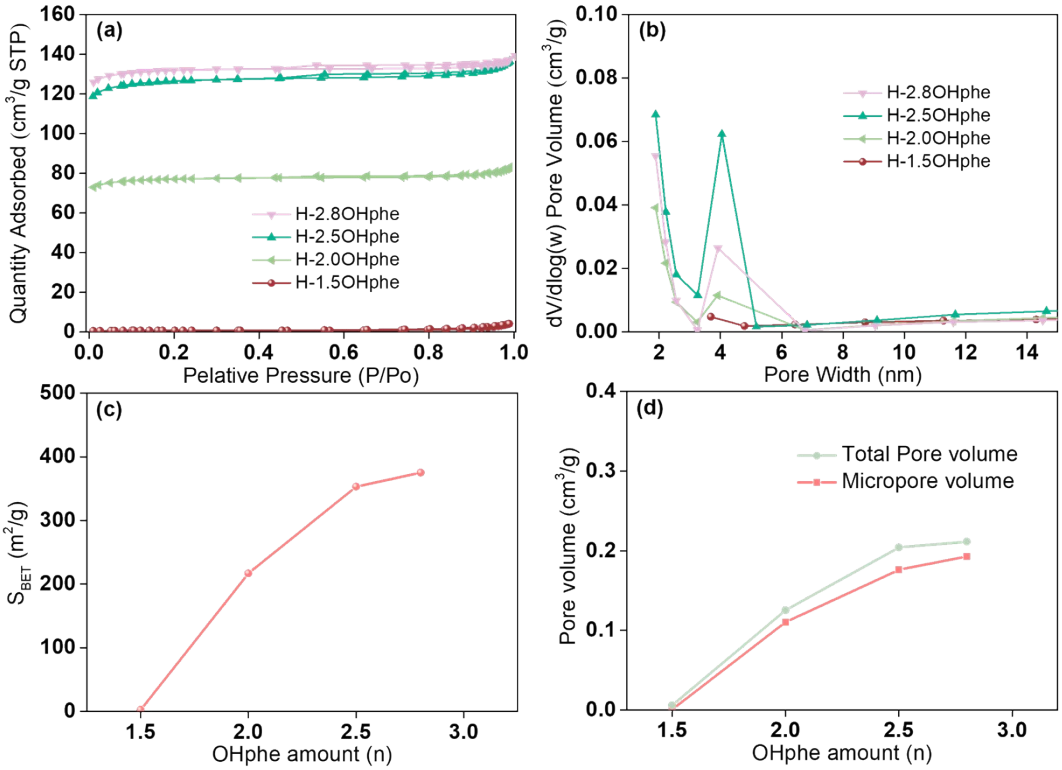

Figure S19. (a) Nitrogen adsorption-desorption isotherms at -196 °C and (b) BJH pore size distribution of hydroquinone-mediated zeolites with different hydroquinone amount after ion exchange to their H-form. (c) BET surface area, and (d) total and micropore volume of the series phenol-mediated zeolites after ion exchange to their H-form, H-nOHphe.

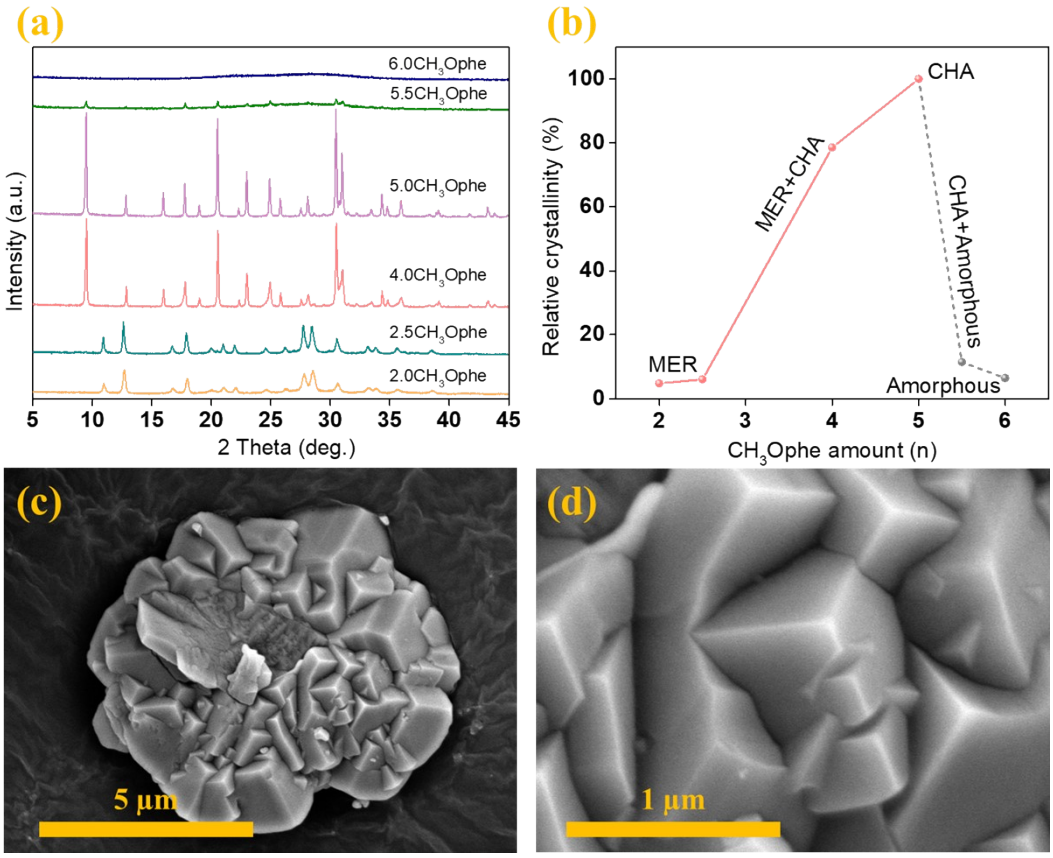

Figure S20. (a) XRD patterns of the as-synthesized K-nCH_3Ophe samples (n = 2.0, 2.5, 4.0, 5.0, 5.5, 6.0), and the (b) relative crystallinity profile of CHA zeolites normalized to that of K-5.0CH_3Ophe as a function of added CH_3Ophe amount. (c-d) SEM images of the as-synthesized K-5.0CH_3Ophe sample, (c) presents a lower magnification overview, while (d) offers a higher magnification detail of the zeolite.

Table S3. The pH of the synthesis mixture with a molar composition of KOH : $Al(OH)_3$: SiO_2 : Ω : H_2O = 7 : 4 : 10 : 3 : 150 (Ω = NH_4F or Clphe) at different crystallization stages.

Stages	pH for Ω = NH_4F	pH for Ω = Clphe
KOH+$Al(OH)_3$	14.82	14.82
KOH+$Al(OH)_3$+SiO_2	14.05	14.05
KOH+$Al(OH)_3$+SiO_2+3.0Ω	13.77	13.64
After aging 24 h	14.13	13.85
After 160 °C 4 days	11.75	10.37

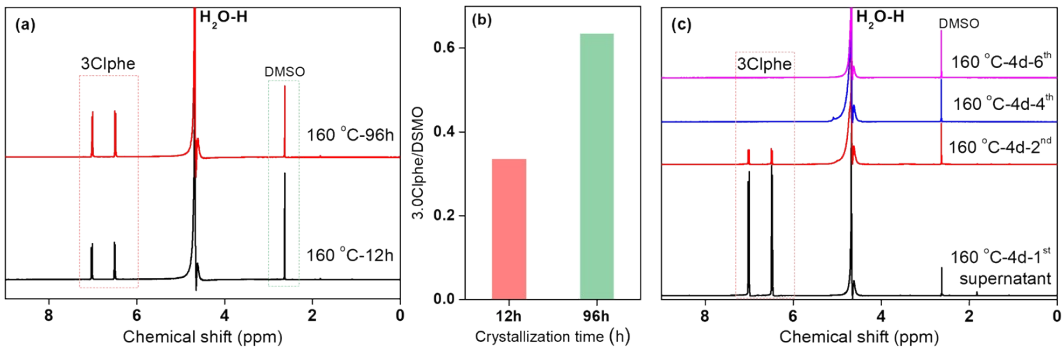

Figure S21. ^{1}H NMR spectra of (a) the reaction mixture for K-3.0Clphe at different crystallization time using dimethyl sulfoxide (DMSO) as an internal standard and (b) the corresponding 3.0Clphe/DMSO ratio, and of (c) the mother liquid collected after different washing cycles of the as-synthesized K-3.0Clphe crystals.

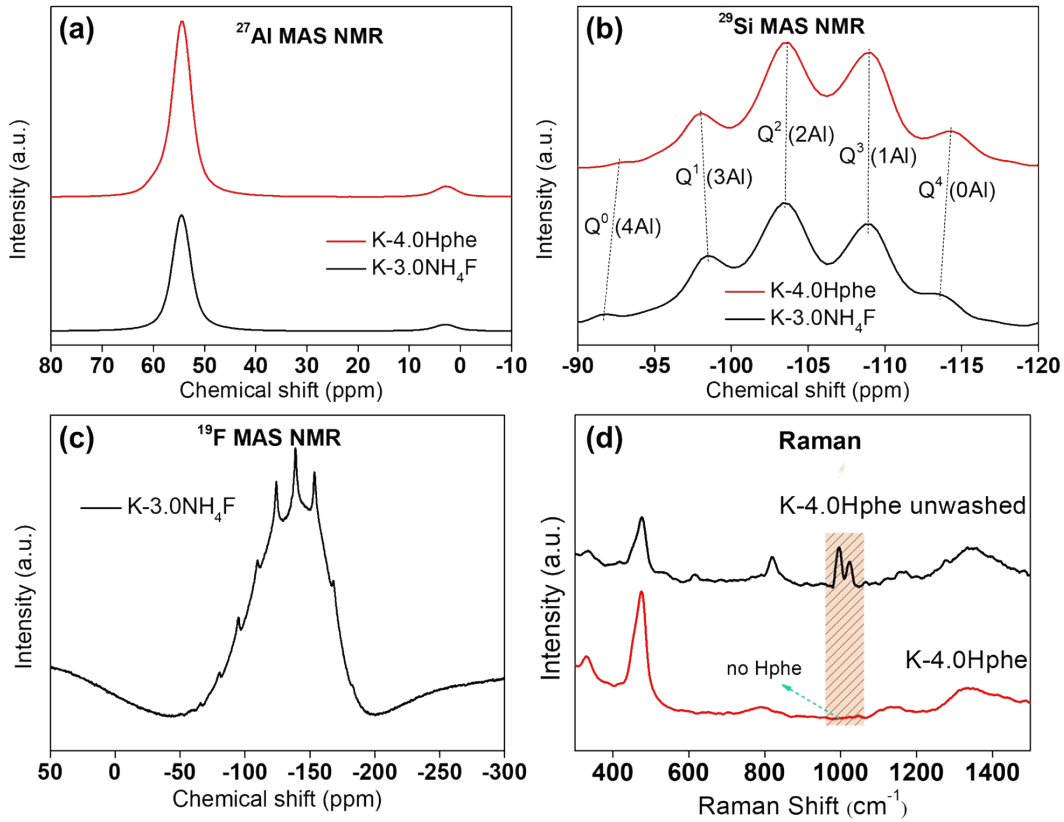

Figure S22. The comparative characterizations of K-3.0NH_4F and K-4.0Hphe. (a) ^{27}Al MAS NMR, (b) ^{29}Si MAS NMR, (c) ^{19}F MAS NMR of K-3.0NH_4F, and (d) Raman spectrum of K-4.0Hphe before and after water washing.

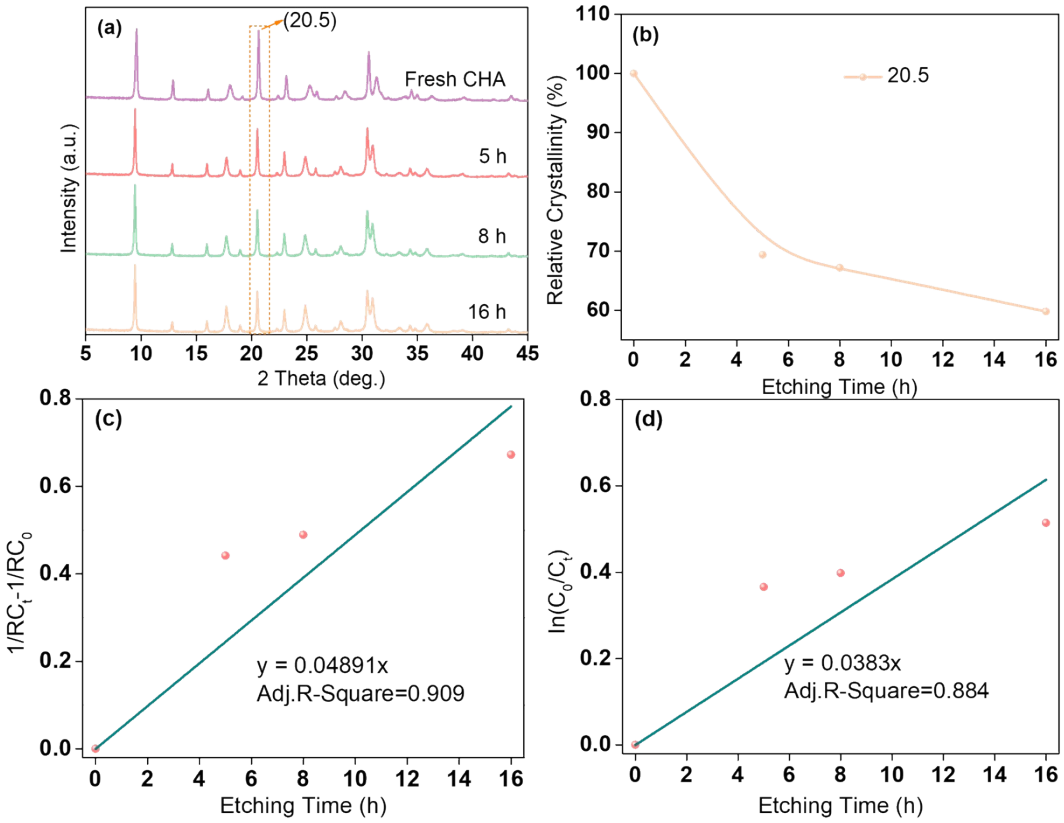

Figure S23. (a) XRD patterns of the K-4.0Hphe samples etched by 1.0 M hydroquinone at 80 °C for various treatment time (t =0, 5, 8, 16 h), and (b) the relative crystallinity profile normalized to that of K-4.0Hphe. The (c) pseudo-second-order and (d) pseudo-first-order dissolution kinetic fit.

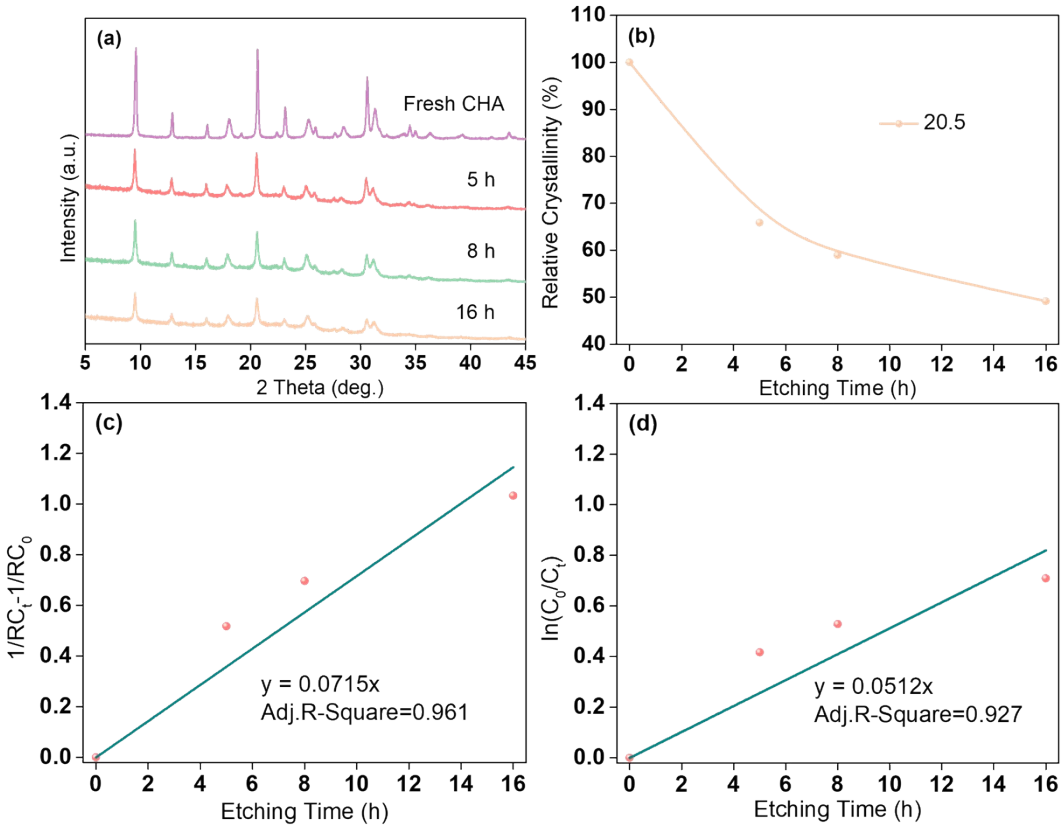

Figure S24. (a) XRD patterns of the K-4.0Hphe samples etched by 1.0 M NH_4F at 80 °C for various treatment time (t =0, 5, 8, 16 h), and (b) the relative crystallinity profile normalized to that of K-4.0Hphe. The (c) pseudo-second-order and (d) pseudo-first-order dissolution kinetic fit.

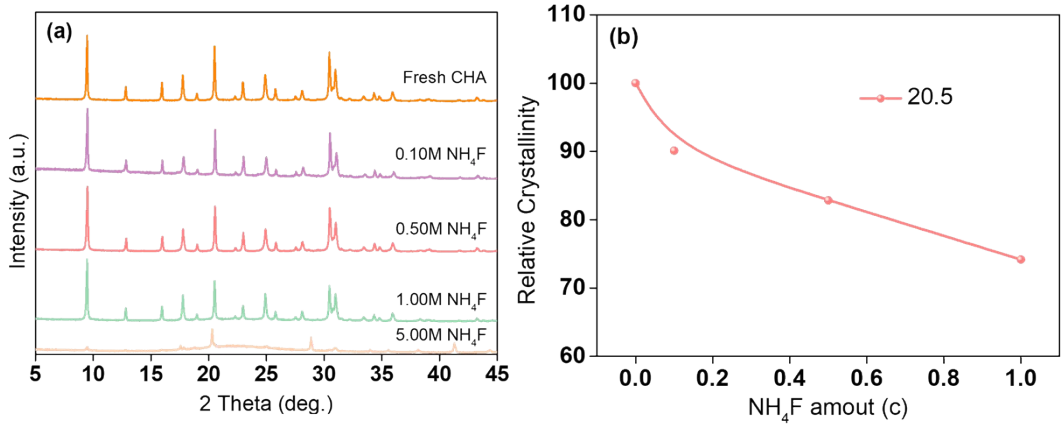

Figure S25. (a) XRD patterns of the K-4.0Hphe samples etched by NH_4F at 80 °C for 8 h at various NH_4F concentration (*c* =0, 0.1, 0.5, 1.0 M), and (b) the relative crystallinity profile normalized to that of K-4.0Hphe.

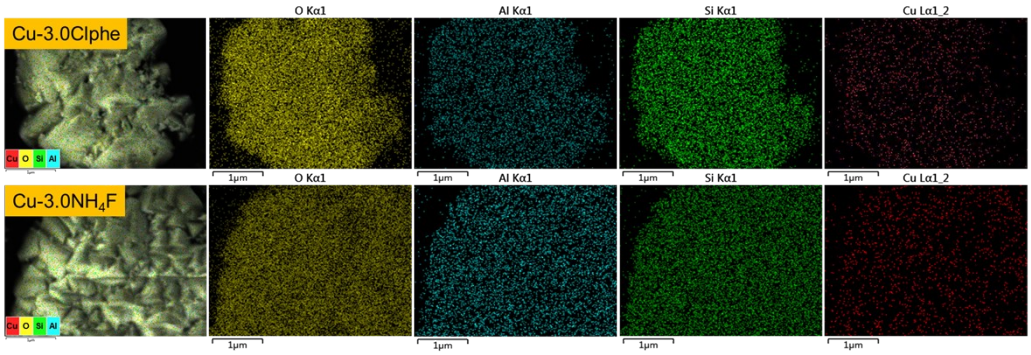

	O At%	Si At%	Al At%	Cu At%	Si/Al
Cu-3.0Clphe	64.5	24.1	9.9	1.4	2.43
Cu-3.0NH_4F	64.7	24.2	10.1	1.0	2.40

Figure 26. SEM images and EDX mappings of Cu-3.0Clphe and Cu-3.0NH_4F catalysts and the corresponding elemental analysis.

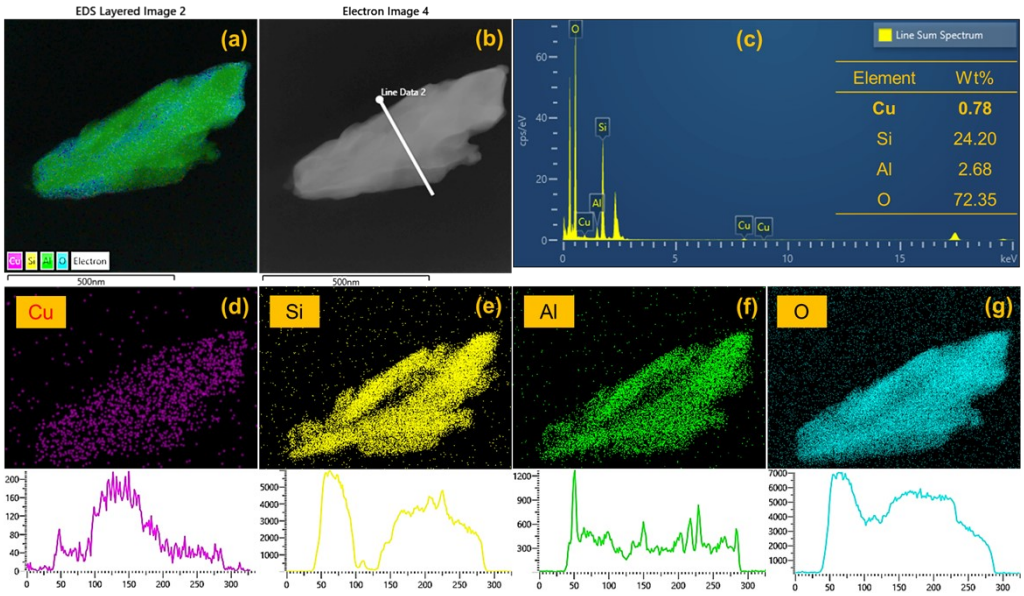

Figure S27. TEM image, EDX mapping and line profiles of Cu-3.0Clphe and the corresponding elemental analysis.

Table S4. Textural properties of the Cu-3.0Clphe and Cu-3.0NH_4F catalysts.

Sample	BET surface area (m^2/g)	Micropore volume (cm^3/g)	Total pore volume (cm^3/g)	Mesopore volume (cm^3/g)
Cu-3.0Clphe	322.37	0.18	0.20	0.02
Cu-3.0NH_4F	302.33	0.16	0.18	0.02

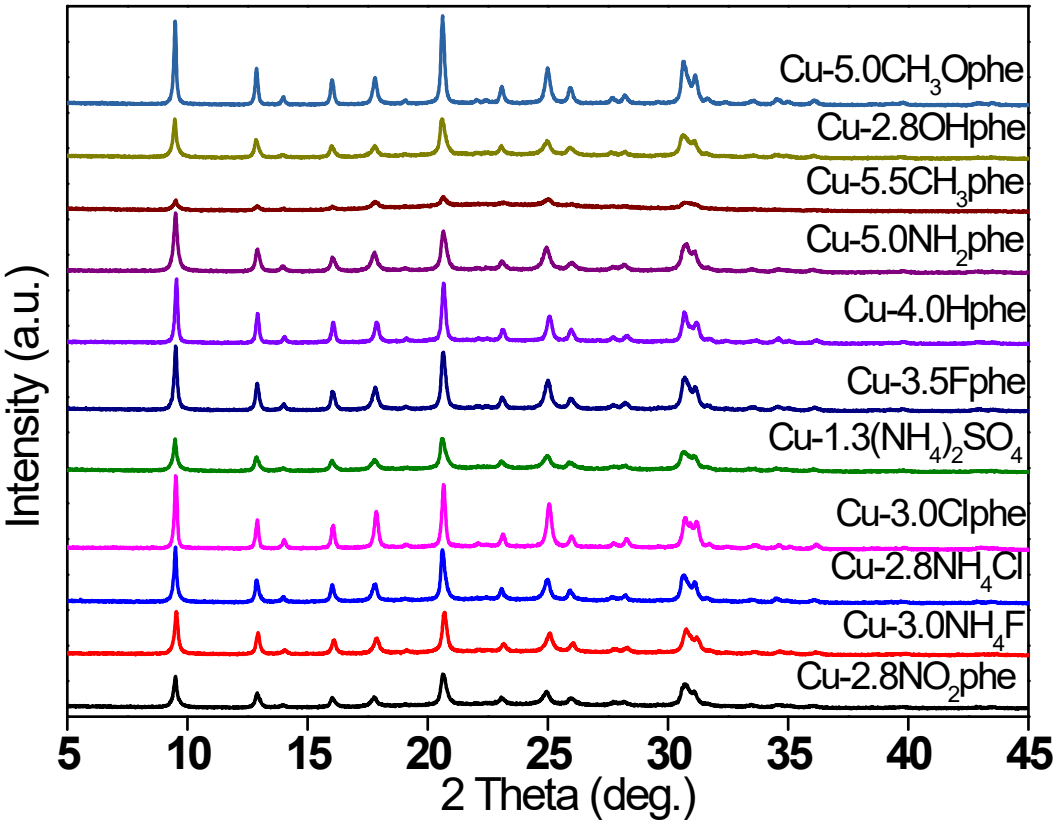

Figure S28. XRD patterns of copper-exchanged Cu-nΩ catalysts.

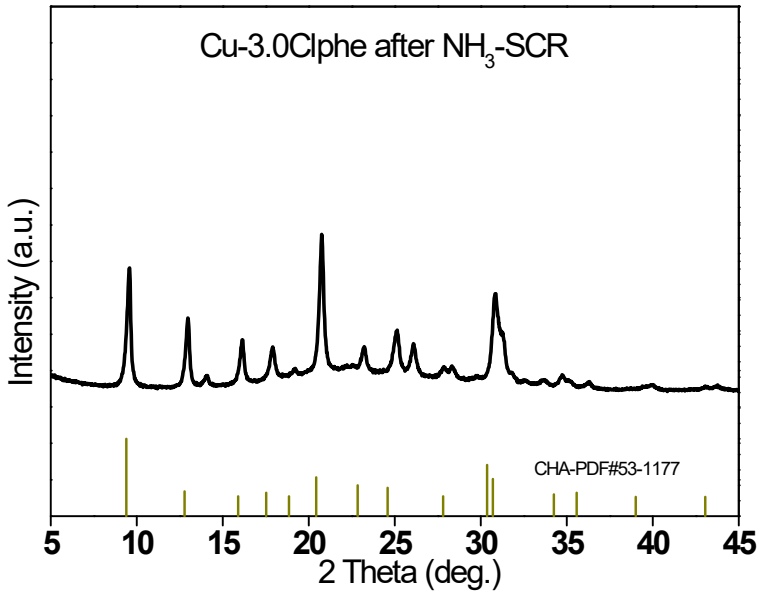

Figure S29. XRD pattern of the spent Cu-3.0Clphe catalyst after NH_3-SCR

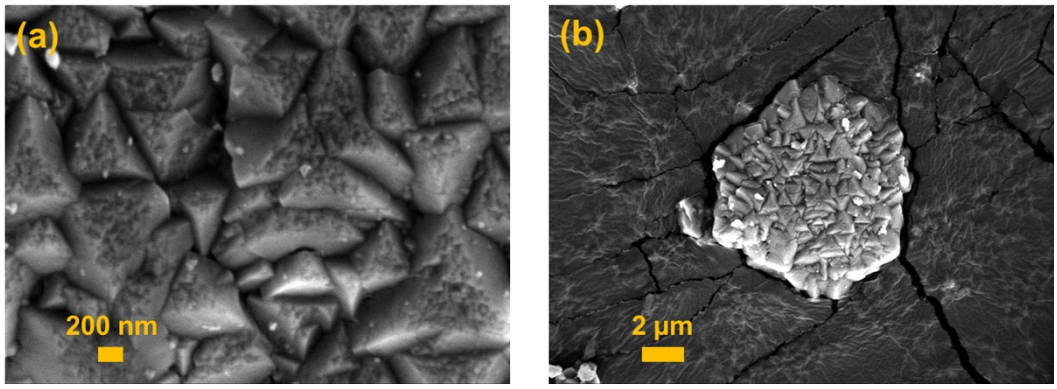

Figure S30. SEM images of the spent Cu-3.0Clphe catalyst after NH_3-SCR

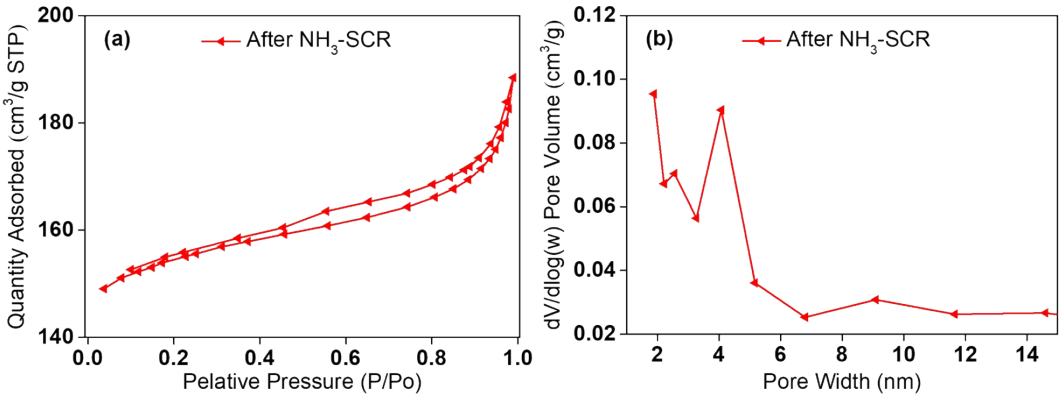

Figure S31. (a) N_2 adsorption-desorption isotherm and (b) the corresponding BJH pore size distribution of the spent Cu-3.0Clphe catalyst after NH_3-SCR

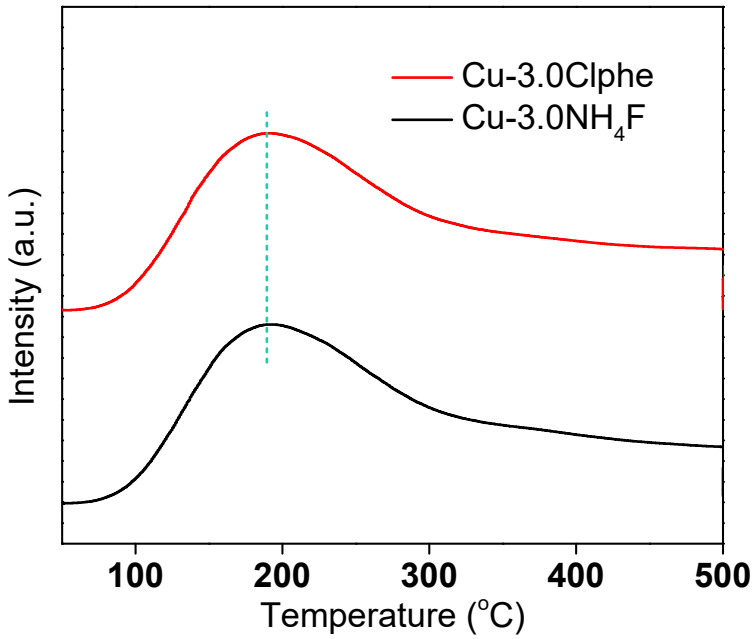

Figure S32. NH_3-SCR catalytic performance of Cu-4.0Hphe catalyst before and after long term hydrothermal aging at 600 °C for 6 h in 5 vol % H_2O

Table S5. Quantitative analyses for H_2-TPR of the Cu-3.0Clphe and Cu-3.0NH_4F catalysts.

Sample	H_2 consumption (μmol/g)
Cu-3.0Clphe	374.90
Cu-3.0NH_4F	236.28

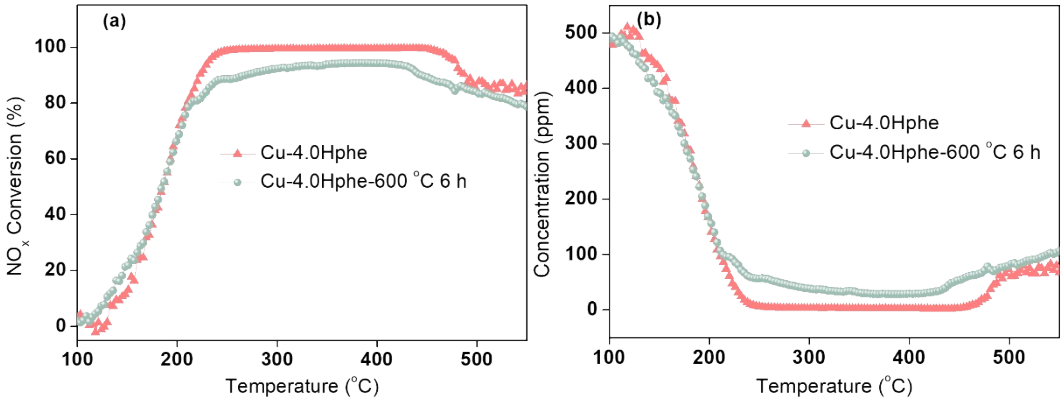

Figure S33. NH_3-SCR catalytic performance of Cu-4.0Hphe catalyst before and after long term hydrothermal aging at 600 °C for 6 h in 5 vol % H_2O